Simultaneous multislice spectral-spatial excitations for reduced signal loss susceptibility artifact in BOLD functional MRI

Simultaneous Multislice Spectral-Spatial Excitations for Reduced Signal Loss Susceptibility Artifact in BOLD Functional MRI

Robert J. Anderson,[1]* Benedikt A. Poser,[1,2] and V. Andrew Stenger[1]

Purpose: Simultaneous multislice (SMS) imaging can significantly increase image acquisition rates and improve temporal resolution and contrast in gradient-echo blood oxygen level–dependent (BOLD) functional MRI (fMRI) experiments. Through-plane signal loss due to B_0 inhomogeneities at air–tissue interfaces limits fMRI of structures near the nasal cavity and ear canals. This study implemented spectral–spatial (SPSP) radiofrequency pulses for reduced through-plane signal loss across multiple simultaneously excited slices.

Theory and Methods: Multiband (MB) and power independent of number of slices (PINS) methods are combined with SPSP excitation for signal loss compensation in slice-accelerated human brain imaging. Nine simultaneous slices of 5-mm thickness and 20 mm apart were excited using standard MB radiofrequency pulses and the proposed SPSP-SMS pulses, yielding coverage of 36 slices in four shots with 350-ms volume pulse repetition time. The pulses were compared in breath-hold fMRI at 3T.

Results: The SPSP-SMS pulses recovered ~45% of voxels with signal loss in standard SMS images. Activation in areas of signal recovery increased by 26.4% using a 12.6-ms SPSP-MB pulse and 20.3% using a 12.1-ms SPSP-PINS pulse.

Conclusions: It is demonstrated that SPSP-SMS pulses can improve BOLD sensitivity in areas of signal loss across simultaneous multiple slices. **Magn Reson Med 72:1342–1352, 2014.** © **2013 Wiley Periodicals, Inc.**

Key words: simultaneous multislice excitation; spectral–spatial excitation; susceptibility artifact correction; BOLD fMRI

INTRODUCTION

Simultaneous multislice (SMS) imaging methods have garnered interest within the MRI community because of the significant reduction in the time required to scan a volume. This is particularly useful in MRI experiments that benefit from higher temporal resolution and greater sampling power. In particular, it has been demonstrated that SMS methods can increase blood oxygen level–dependent (BOLD) functional MRI (fMRI) acquisition speeds by factors of four and greater (1–4). This translates into increased statistical power in the activation analysis (5) and a better ability to identify nuisance physiological signal components (6). The most common method of achieving SMS excitations is with a multiband (MB) radiofrequency (RF) pulse, where the waveform of a single slice is phase-modulated with multiple frequencies and then recombined linearly. Recently, power independent of number of slices (PINS) RF pulses were introduced as another approach to SMS excitation (7). PINS pulses require approximately factor N lower peak RF power to excite the same number of slices compared with its corresponding MB pulse. However, PINS pulses excite an infinite train of equidistant slices due to a small field of excitation (FOX).

Gradient echo BOLD fMRI in the lower brain remains challenging due to susceptibility induced signal loss. The signal loss is particularly problematic in the through-plane direction in axial slices due to the proximity of inferior air cavities. There have been several methods proposed to mitigate the signal loss due to susceptibility effects. Among these are z-shim methods (8), thin slice averaging (9), shim coils (10), multi-echo sequences (11), parallel transmission (12), and tailored RF pulses (13). Methods that can achieve signal loss corrections in a single excitation are of particular importance in the fMRI context because they do not increase scan time. Spectral–spatial (SPSP) pulses have recently been shown to be capable of reducing the signal loss artifact in a single excitation (14–16). Such pulses are designed to have a SPSP excitation with a frequency-dependent through-plane phase pattern, which is equal and opposite to that produced by the magnetic susceptibility at echo time T_E. By exciting with a precompensated phase, a phase-coherent signal at the center of k-space is created at T_E and thus recovers the majority of the original signal. Crucially, only off-resonance components will be corrected, meaning that the excitation is equivalent to that of a standard pulse in regions with little or no off resonance. Because of this, SPSP pulses can be used to simultaneously excite numerous slices compensated for signal loss across the entire volume of the brain.

THEORY

Susceptibility Artifact Correction with Spectral-Spatial Pulses

Signal loss artifact arises from through-plane variations in the magnetic susceptibility at the interface between air and tissue. During the time between the excitation and the acquisition of the center of k-space, the excited spins will develop inhomogeneous phases that result in

[1]Department of Medicine, John A. Burns School of Medicine, University of Hawaii, Honolulu, Hawaii, USA.

[2]Department of Cognitive Neuroscience, Faculty of Psychology and Neuroscience, Maastricht University, Maastricht, The Netherlands.

Grant sponsor: National Institutes of Health; Grant numbers: R01DA019912, R01EB011517 and K02DA020569; Grant sponsor: German Research Foundation; Grant number: Po1576/1-1.

*Correspondence to: Robert J. Anderson, Ph.D., University of Hawaii JABSOM, The Queen's Medical Center, 1356 Lusitana Street, 7th floor, Honolulu, HI 96813. E-mail: rjanders@hawaii.edu

Received 15 July 2013; revised 25 October 2013; accepted 28 October 2013

DOI 10.1002/mrm.25050

Published online 12 December 2013 in Wiley Online Library (wileyonlinelibrary.com).

cancellations during data readout. This results in signal loss artifacts characterized by large signal voids in the images. It has previously been shown that SPSP pulses are capable of mitigating this signal loss by pre-compensating the slice with an equal and opposite frequency-dependent through-plane phase. In these pulse designs, the through-plane susceptibility gradient was modeled using a linear relationship $G_s(f) = \alpha f$ with value α measured to be on the order of -1.0 μT/m/Hz in the typical human brain (17). At T_E, the phase of a given spin will then be both z- and f-dependent: $\phi_s(z,f) = \gamma G_s(f) z T_E = \gamma\alpha f z T_E$.

An SPSP pulse can be designed using the small tip-angle approximation (18), where an excitation of duration T can be thought of as a time-symmetric analogue to acquisition and the resulting magnetization profile is the Fourier transform of the RF pulse $B(t)$:

$$M(z)e^{-\gamma\alpha f z T_E} = \int_0^T B(t)e^{-i(k_z(t)z + k_f(t)f)}dt. \quad [1]$$

Here, the corresponding excitation k-space trajectories differ only in that they are time-reversed: $k_z(t) = \gamma\int_t^T G_z(s)ds$ and $k_f(t) = T - t$, with gyromagnetic ratio γ and slice-select gradient G_z. Note that the excited slice magnetization $M(z)$ is pre-compensated for the frequency dependent through-plane susceptibility gradient. An SPSP pulse typically achieves spatial localization with slice-select subpulses consisting of a trapezoidal gradient and RF waveform $p(t)$, which is the inverse Fourier transform of $P(z)$, the desired slice profile along z that has slice thickness z_0. An infinite number of distinct frequency bands are produced by repeating the subpulses H times per excitation (19). The resolution of the frequency bands will be proportional to $1/H$. The separation stop-band f_s between aliased frequency bands will be determined by $1/T_{\text{sub}}$, where T_{sub} is the time between each subpulse. One can either alternate the gradient polarity of each subpulse and put the gradient rewinder at the end or keep the gradient polarities the same and include a rewinder with each subpulse. The latter is known as the "fly-back" design and is less susceptible to timing errors due to eddy currents than its dual-polarity counterpart (20).

In this study, a design approach was taken whereby the final RF pulse was obtained by the complex summation of J number of SPSP pulses that each produce the desired through-plane phase pre-compensation for the j^{th} frequency band centered at $j\Delta f$(21) , where Δf is the frequency sampling step size. Placing each pulse at the proper spectral position is done so by phase-modulating $p(k_z(t))$ by $j\Delta f$. The through-plane phase pre-compensation for a given frequency band is introduced by shifting the center of the k-space of its waveform, which is equivalent to unbalancing the slice-select gradient thus creating a z-shim. The shift for a given TE and Δf is $\Delta k = \gamma\alpha\Delta f T_E$. The final form of the SPSP pulse is obtained by summing over the frequency bands:

$$B_{\text{SPSP}}(t) = w(t)\sum_{j=-J/2+1/2}^{J/2-1/2} p_j(k_z(t) + j\Delta k)e^{i2\pi j\Delta f(T-t)+i\theta_j}. \quad [2]$$

Here $w(t)$ is a temporal weighting function applied to the entire pulse to smooth the spectral profile of each frequency band. Its Fourier transform is $W(f)$, the width of which will determine the passband f_p of the pulse. The term θ_j is an adjustable constant phase, which is set such that the bands have the same phase in regions where they overlap.

Evaluating Equation 1, the magnetization profile of the SPSP pulse is:

$$M_{\text{SPSP}}(z,f) = P(z)W(f) * \sum_{j=-J/2+1/2}^{J/2-1/2} \delta(f - j\Delta f)e^{-i\gamma\alpha j\Delta f T_E z + i\theta_j}. \quad [3]$$

The magnetization will be comprised of a series of overlapping frequency bands each with a unique through-plane phase pre-compensation. Note that only the central frequency passband, which will have a net width of approximately $J\Delta f$, is being considered here.

MB SMS Excitation

SMS excitation is typically achieved using an MB RF pulse, a modulated single-slice waveform that produces N slices with separation Δz. For slices symmetric about the isocenter, this is written as:

$$B_{\text{MB}}(t) = p(k_z(t))\sum_{n=-N/2+1/2}^{N/2-1/2} e^{2i\pi k_z(t)n\Delta z}. \quad [4]$$

The corresponding magnetization is:

$$M_{\text{MB}}(z) = P(z) * \sum_{n=-N/2+1/2}^{N/2-1/2} \delta(z - n\Delta z). \quad [5]$$

Because an MB pulse is merely the linear superposition of N-modulated waveforms, the peak RF voltage of an MB pulse will increase linearly with N and can restrict practical implementation of MB pulses due to hardware limitations. Furthermore, peak power is proportional to the square of the peak voltage, and therefore will increase by a factor of N^2, while the amount of specific absorption rate (SAR) experienced by the subject follows the time integral of square of the voltage and thus increases with N.

PINS SMS Excitation

If peak RF power or SAR is a concern, the PINS technique, a series of nonselective pulses separated by gradient z-blips, is a useful alternative. The distinguishing characteristic of a PINS pulse is that these z-blips are designed such that the FOX is relatively small. In this manner, multiple slices are simultaneously excited with separation Δz being equal to the FOX. The number of effectively excited slices is not an independent variable and is determined by the dimension of the RF coil and the subject dimensions along the slice direction. From an excitation k-space perspective, a PINS pulse can be constructed by first selecting the appropriate area for the z-blip:

$$A_{\text{blip}} = \frac{2\pi}{\gamma \Delta z}. \quad [6]$$

This z-blip is repeated multiple times in order to create a k-space trajectory that can provide sufficient resolution along the slice-select direction. Interspersed between the z-blips are rectangular RF subpulses, which are weighted by $p(k_z(t))$ along the whole PINS pulse:

$$B_{\text{PINS}}(t) = p(k_z(t))\text{rect}(t/t_0)\sum_{l=0}^{L}\delta(t - l(t_0 + t_{\text{blip}}) - t_0/2). \quad [7]$$

Here, L is the total number of z-blips and t_{blip} is the duration of each. The time t_0 between subsequent z-blips also corresponds to the length of an individual RF rectangular subpulse. The parameter t_0 can be adjusted to either minimize the overall pulse length or the required peak RF voltage. The magnetization generated by a PINS pulse is:

$$M_{\text{PINS}}(z) = P(z) * \sum_{n=-\infty}^{\infty}\delta(z - n\Delta z). \quad [8]$$

SPSP-SMS Pulse Designs

The SPSP-MB pulse is constructed from Equations 2 and 4:

$$B_{\text{SPSP-MB}} = w(t)\sum_{j=-J/2+1/2}^{J/2-1/2} p(k_z(t) + j\Delta k)e^{i2\pi j\Delta f(T-t)+i\theta_j} \times \sum_{n=-N/2+1/2}^{N/2-1/2} e^{i2\pi k_z(t)n\Delta z}. \quad [9]$$

Likewise, Equation 10, the corresponding expression for the SPSP-PINS pulse, is formed by combining Equations 2 and 7 and repeating H number of times:

$$B_{\text{SPSP-PINS}}(t) = w(t)\sum_{j=-J/2+1/2}^{J/2-1/2} p(k_z(t) - j\Delta k)e^{i2\pi j\Delta f(T-t)+i\theta_j} \text{rect}(t/t_0)\sum_{h=0}^{H-1}\sum_{l=0}^{L}\delta(t - (l(t_0 + t_{\text{blip}}) + t_0/2 + hT_{\text{sub}}))$$

where T_{sub} is the duration of a single PINS subpulse, including any rewinding gradients. Finally, the magnetization generated by these pulses can be written as:

$$M_{\text{SPSP-MB}} = [P(z)W(f)] * * \left[\sum_{n=-N/2+1/2}^{N/2-1/2}\delta(z - n\Delta z) \sum_{j=-J/2+1/2}^{J/2-1/2}\delta(f - j\Delta f)e^{-i\gamma\alpha j\Delta f T_E z + i\theta_j}\right] \quad [10]$$

and

$$M_{\text{SPSP-PINS}} = [P(z)W(f)] * * \left[\sum_{n=-\infty}^{\infty}\delta(z - n\Delta z) \sum_{j=-J/2+1/2}^{J/2-1/2}\delta(f - j\Delta f)e^{-i\gamma\alpha j\Delta f T_E z + i\theta_j}\right]. \quad [11]$$

METHODS

Pulse Design

MATLAB (Mathworks, Natick, Massachusetts, USA) was used to create fly-back SPSP-MB and SPSP-PINS pulses with $p(k_z(t)) = \text{sinc}(k_z(t))$ and peak slew rates of 150 mT/m, peak gradients of 30 mT/m, and a sampling resolution of 10 μs. In order to create a smooth phase pattern, $J = 5$ frequency bands were placed with $\Delta f = 60$ Hz. These values were chosen via visual inspection of the simulated SPSP profiles. A value of $T_E = 35$ ms was used to calculate the k-space shift Δk for $\alpha = -1.0$ mT/m/Hz. The SPSP-MB pulse consisted of six subpulses (2.14 ms each, $f_s \approx 470$ Hz) designed to excite $N = 9$ slices with thickness $z_0 = 5$ mm and separation $\Delta z = 20$ mm. A 10 mT/m excitation gradient was used during the application of the RF waveform, while the peak gradient value was used for the fly-back portion of each subpulse. From a frequency perspective, this resulted in a separation of 8500 Hz between adjacent slices. The temporal weighting function $w(t)$ was chosen such that $f_p \approx 120$ Hz and had a Gaussian shape. The total pulse duration was 12.62 ms. The SPSP-PINS pulse was composed of four subpulses (3.06 ms each, $f_s \approx 325$ Hz) comprising ten 180-μs z-blips interleaved with $t_0 = 60$ μs rectangular RF pulses. In the case of PINS, the frequency separation between adjacent slices is determined directly by the inverse of the time interval between RF pulses, and in this case was 4170 Hz. In other respects, it was comparable to the SPSP-MB pulse: $\Delta z = 20$ mm, $z_0 = 5$ mm, 10 mT/m excitation gradient, $f_p \approx 130$ Hz, and total duration $T = 12.06$ ms. The number of subpulses was chosen such that both pulses were approximately the same length. Figure 1 plots the real and imaginary RF components of the SPSP-MB (Fig. 1A) and SPSP-PINS (Fig. 1B) pulses described here, along with their respective slice-select gradients G_z. The magnetization profiles $M(z,f)$ produced by the pulses were examined via Bloch equation simulations which were also ran in MATLAB.

Human Brain Imaging

Images of the human brain were acquired in four normal adult subjects using a Siemens TIM Trio VB17 3T scanner (Siemens Healthcare, Erlangen, Germany) after informed consent and approval by the University of Hawaii and Queens Medical Center joint Institutional Review Board. In each subject, four whole brain scans were acquired using 1) a single-slice sinc pulse, 2) a standard $N = 9$ MB (Standard-MB) pulse, 3) the $N = 9$ SPSP-MB pulse, and 4) the SPSP-PINS pulse. The MB parameter $N = 9$ was chosen such that these pulses would excite approximately the same slices as the PINS pulse. In all scans, 36 slices were acquired such that the SMS acquisitions required four excitations per volume. For the SMS acquisitions, a blipped-CAIPI EPI sequence

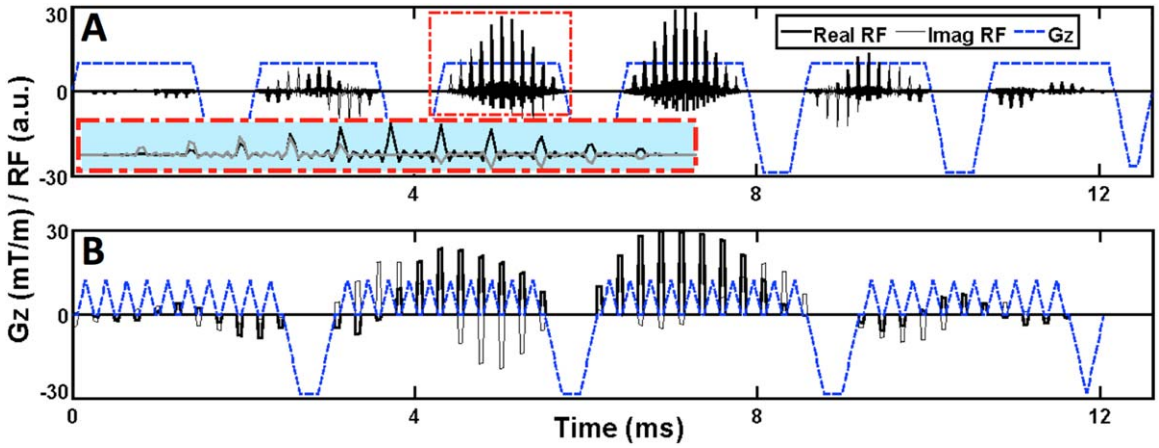

FIG. 1. Diagrams showing the real and imaginary RF waveforms and slice-select gradient of the SPSP-MB (**A**) and SPSP-PINS (**B**) pulses. The SPSP-MB pulse consists of six 2.14 ms MB subpulses and has a total duration of 12.62 ms. Four 3.06 ms PINS subpulses, each comprising ten G_z blips interleaved with eleven 60-μs hard RF pulses, produce an SPSP-PINS pulse 12.06 ms long. [Color figure can be viewed in the online issue, which is available at wileyonlinelibrary.com.]

(4) was implemented (pulse repetition time [TR] = 350 ms; TE = 36 ms; flip angle [FA] = 37°; in-plane resolution = 96 × 96; field of view [FOV] = 240 mm; 2.5 × 2.5 × 5 mm^3 voxels, CAIPI shift FOV/3). Single-slice reference images were acquired for the calculation of slice-GRAPPA (22) kernels with kernel size 3 × 4, which were then used for the reconstruction of all SMS scans. A standard 2D EPI sequence with TR = 1400 ms and otherwise identical parameters was used for the single-slice acquisitions. The Siemens body transmission coil and 32-channel receiver coil were used for all scans.

The ability for the SPSP-SMS pulses to recover lost signal were quantitatively assessed by first determining the regions in the Standard-MB images that were below 10% of their normalized maximum intensities. These voids were taken to represent voxels where the SPSP pulses had the potential to have a meaningful effect. The SPSP-SMS pulse image voxels that both had magnitudes above their respective 10% thresholds and were located in the void regions were then counted, and the total percentages of the recovered voxels within the voids were calculated. Difference images were also calculated for qualitative purposes. Subtracting the normalized Standard-MB image volume from the two SPSP-SMS image volumes created these difference maps. Three-voxel by three-voxel in-plane smoothing and windowing between 5% and 20% change, relative to the maximum image intensity, was performed on the difference images.

Functional MRI Experiments

Three 5-min fMRI breath-hold experiments, consisting of a 20-s breathing/20-s breath-holding paradigm, were also performed for each subject using the same sequence parameters as above. Breath-holding fMRI creates a relatively large BOLD contrast throughout the whole brain and is useful for evaluating methodology. In addition to scanning with each of the two SPSP-SMS pulses, uncorrected control data with the same temporal resolution was acquired with the Standard-MB pulse. FSL (FMRIB,

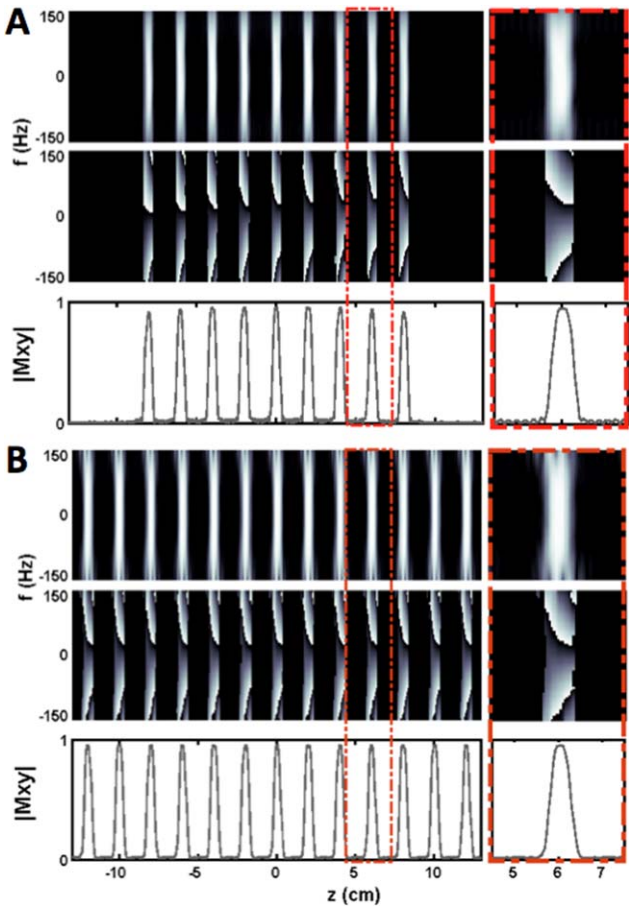

FIG. 2. Bloch equation simulations of the SPSP-MB (**A**) and SPSP-PINS (**B**) pulses. The magnitude (top) and phase (middle) of the transverse magnetization, as a function of z and f, are plotted for 26-cm FOV_z (left) and a single slice (right). The on-resonance profile of the magnitude along z is shown in the bottom panel. Compared with each other, the pulses produce very similar excitations. [Color figure can be viewed in the online issue, which is available at wileyonlinelibrary.com.]

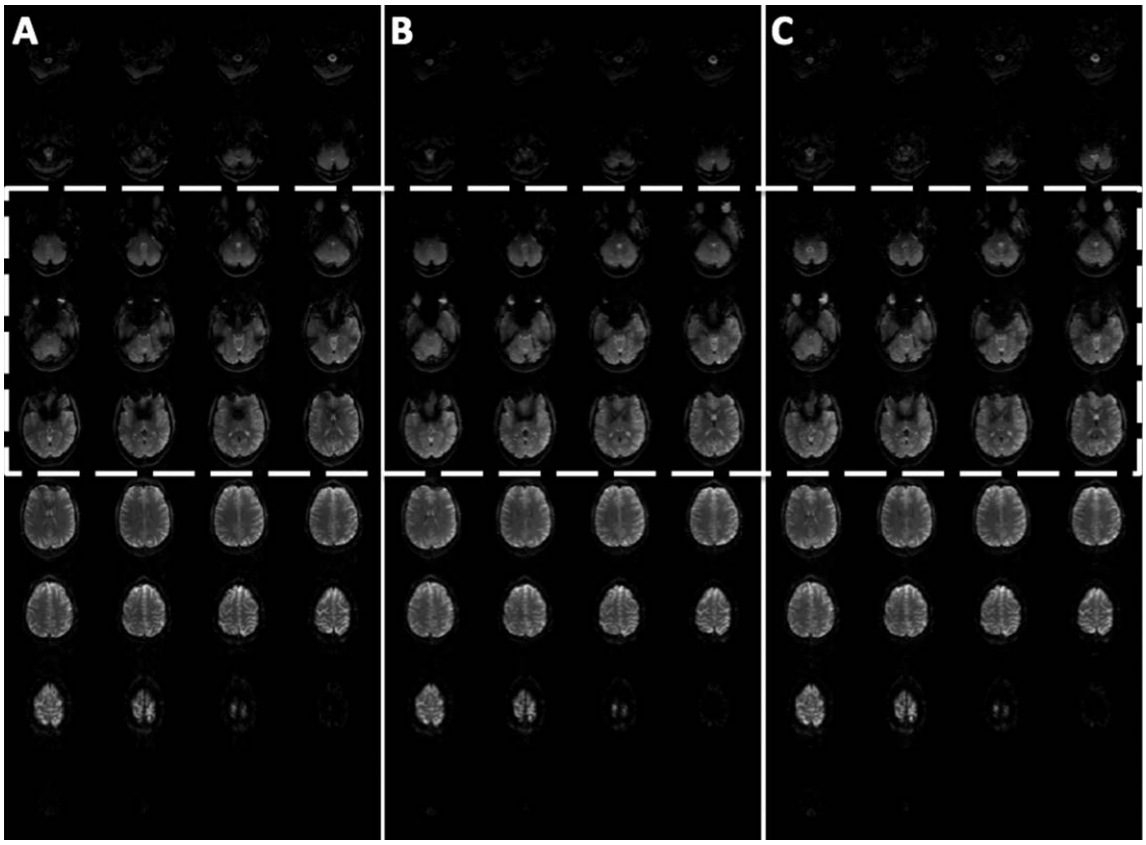

FIG. 3. Human brain images acquired at 3T using the Standard-MB (**A**), SPSP-MB (**B**), and SPSP-PINS (**C**) pulses. Each column of nine slices was excited and acquired simultaneously and then separated via slice-GRAPPA reconstruction. The images excited with the Standard-MB pulse show signal loss noticeable particularly in the slices that contain the orbital frontal and inferior temporal regions near the nasal cavity and ear canals, as indicated by the dashed lines.

Oxford, UK) was employed to analyze the fMRI data with the FMRI Expert Analysis Tool (FEAT) (23–25) and the following preprocessing protocols: MCFLIRT motion correction (26,27), BET brain extraction (28), 5-mm full-width-half-max spatial smoothing, and FILM prewhitening (29). Each voxel time series was fit with a boxcar function convolved with the double-gamma hemodynamic response function. Motion parameters were also included in the model. The resulting activation maps were clustered with a Z-stat threshold of 2.3 and cluster P threshold of 0.05 (30).

Two regions of interest (ROI) were used in the quantitative analysis of the effect of using SPSP-SMS pulses in fMRI experiments. The first, ROI-1, was determined directly by the voxels exhibiting significant recovery in the human brain imaging analysis above. ROI-2 was then defined as the remaining volume of the brain outside of ROI-1. Activation coverage in both ROIs was calculated by determining the percentage of their respective volumes that contained voxels with Z-stat $\geq$2.3. The quantity of interest was the change in activation coverage when using SPSP-SMS versus Standard-MB pulses.

SPSP-MB Pulse Slice Thickness Comparison

In order to find out how SPSP-SMS pulses might translate to applications requiring thinner slices, a comparison of signal recovery as a function of slice thickness was performed for the SPSP-MB pulse design. Six pulses for $N=7$ were constructed with slice thicknesses ranging from 2.5 to 5.0 mm in steps of 0.5 mm. A pulse was first designed for 2.5 mm with the following parameters: 180 mT/m peak slew rate, 30 mT/m peak gradient, $J=5$, $\Delta f=70$ Hz, $T_E=36$ ms, $\alpha=-1.0$ mT/m/Hz, six 2.14 ms subpulses, $\Delta z=20$ mm, 18.2 cm FOX, $f_s \approx 455$ Hz, and $f_p \approx 120$ Hz. The total length of the pulse was 12.9 ms. The remaining five pulses with increasing slice thicknesses were then constructed by decreasing the excitation gradient while keeping its duration constant. This was done such that they would have identical parameters other than the slice thickness. Four normal human subjects were scanned after informed consent using the blipped-CAIPI EPI sequence and reconstruction described above. A total of 28 slices were acquired in each subject. Signal recovery using the SPSP-MB pulses was calculated using the human brain imaging analysis method described previously.

RESULTS

Simulations

Figure 2 shows Bloch equation simulations (FA = 90°) of the transverse magnetization and prephasing patterns for

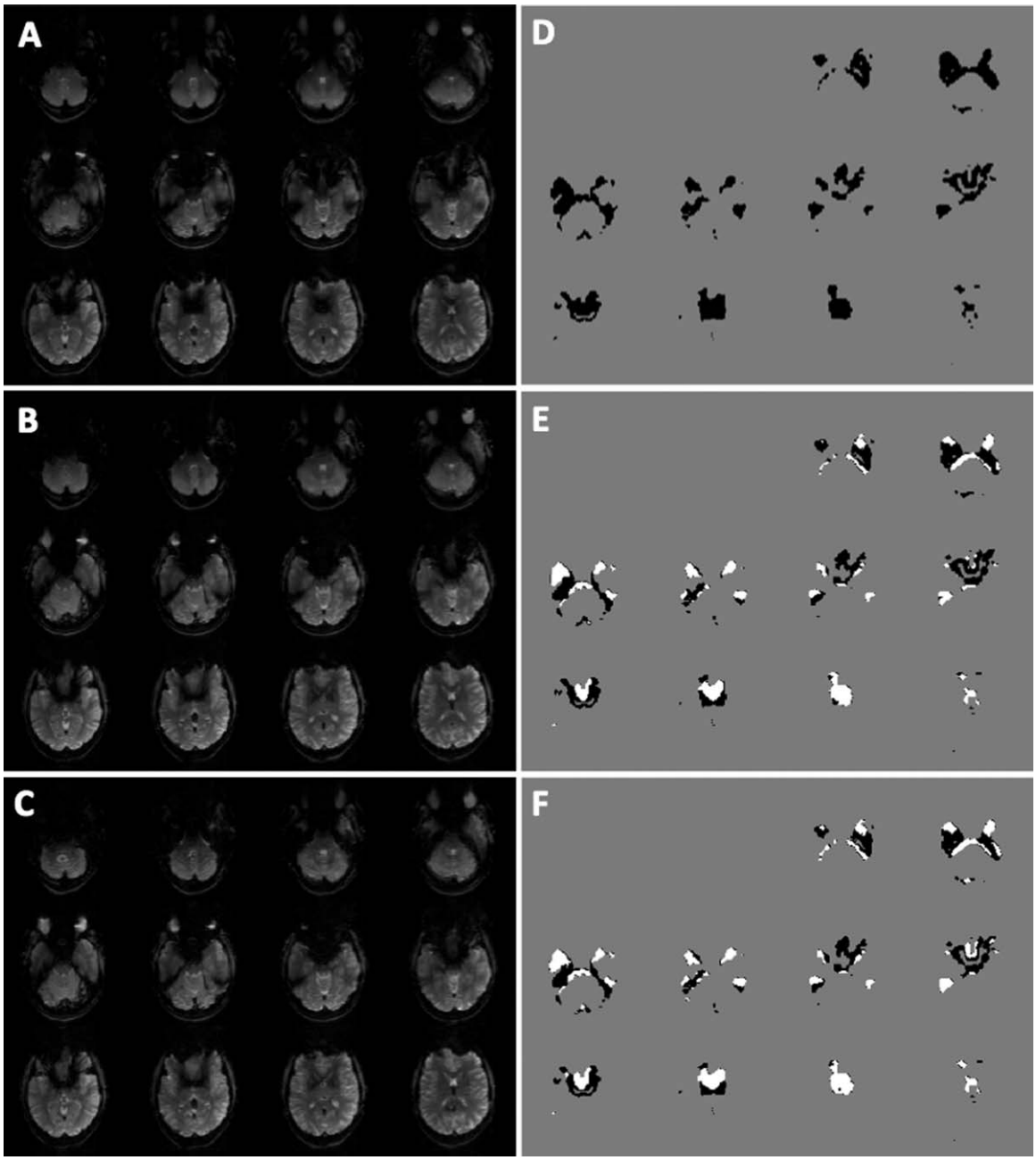

FIG. 4. The three slice groups most affected by the susceptibility artifact are plotted for the Standard-MB (**A**), SPSP-MB (**B**), and SPSP-PINS (**C**) pulses, corresponding to the dashed box in Figure 3. The effect of the SPSP pulses can be easily identified on visual inspection. **D:** The black region maps the voxels in panel A below 10% of the maximum image intensity. **E, F:** The SPSP-MB (E) and SPSP-PINS (F) pulses both affected recovery above 10% for a significant number of these voxels, indicated by white voxels.

Table 1
Percent of Voxels <10% of the Normalized Maximum Intensity in Standard-MB Pulse Images Recovered by SPSP-SMS Pulses and Percent of Voxels in the Brain Included in the Recovery Region

	Subject				Weighted
	1	2	3	4	Average
SPSP-MB, % recovered	47.0	37.6	40.1	45.9	43.3
SPSP-PINS, % recovered	52.1	46.8	40.1	51.8	48.8
Voxels in recovery region, %	3.3	1.8	1.0	3.0	2.2

the SPSP-MB (A) and SPSP-PINS (B) pulses in the frequency range between −150 and +150 Hz across a 26-cm FOV_z on the left, with a single slice FOV_z on the right. Also shown is the on-resonance magnetization profile along z. The overall results are comparable for the two pulses. As expected, the SPSP-PINS pulse excites periodic slices across the entire FOV_z and the SPSP-MB pulse only produces $N = 9$ slices centered about isocenter. Both phase patterns are very good approximations of the target phase pattern [see Fig. 2 in Yip et al. (14)].

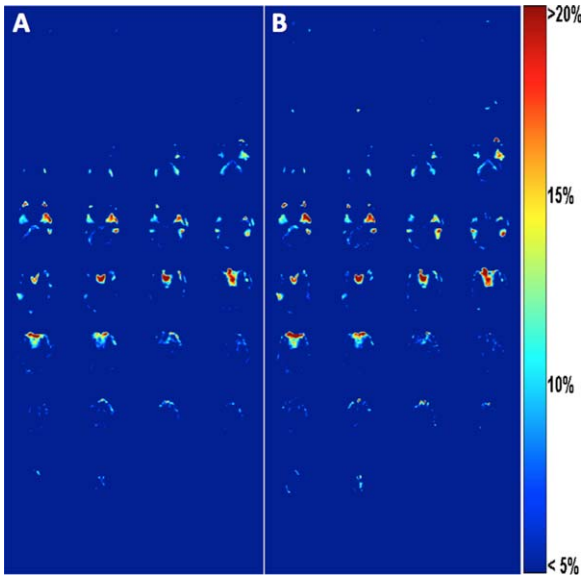

FIG. 5. Difference images created by subtracting the Standard-MB pulse image volume from the SPSP-MB (**A**) and SPSP-PINS (**B**) pulse image volumes provide an alternate perspective on the regions affected by the SPSP pulses. It can be seen that their effect extends into the sixth slice row, a fact not necessarily discernible upon visual inspection of Figure 3 or Figure 4. Both SPSP-SMS pulses have very similar recover patterns. [Color figure can be viewed in the online issue, which is available at wileyonlinelibrary.com.]

Each slice excited by SPSP-PINS is identical in all aspects, regardless of its position relative to isocenter. The SPSP-MB, however, shows some small decrease in the maximum magnitude of the slices far from isocenter. This was due to a slight undersampling of the RF waveform using the 10-μs dwell time, which was used instead of a smaller dwell time due to hardware limitations.

Human Brain Imaging

Figure 3 shows the brain volumes consisting of 36 slices acquired in a representative subject for each of the three SMS experiments using Standard-MB (Fig. 3A), SPSP-MB (Fig. 3B), and SPSP-PINS (Fig. 3C) pulses. Sets of the nine simultaneously excited slices correspond to each column in the figure. The Standard-MB slices contain regions that suffer from signal loss due to susceptibility variations in the vicinity of the nasal cavity and the ear canals. This is indicated by the dashed white line. The signal recovery due to the SPSP-SMS pulses can be observed in the corresponding areas in Figure 3B and 3C. Figure 4 shows the slices within the dashed white line in more detail for the Standard-MB (Fig. 4A), SPSP-MB (Fig. 4B), and SPSP-PINS (Fig. 4C) experiments. The region below the 10% threshold in Figure 4A is mapped by the black voxels in Figure 4D and is where the efficacy of the SPSP-SMS pulses are evaluated. This same region is plotted in Figure 4E and 4F, where white indicates voxels that have been successfully recovered by SPSP-MB and SPSP-PINS, respectively. The quantitative analysis is derived from the number of black and white voxels, while the white voxels are also used to define ROI-1 in the fMRI section. Table 1 displays the signal recovery results for the SPSP-MB and SPSP-PINS pulses for the four subjects along with the average percent of recovered signal. The relative percent of the brain that comprises the recovery regions is also included. It is seen that both SPSP pulses reliably recover around 45% of the reduced signal, with SPSP-PINS slightly outperforming SPSP-MB by this metric.

Figure 5 shows the difference images derived from Figure 3, used here for visualization purposes. The increases in intensity when using the SPSP-MB pulse as opposed to the Standard-MB pulse are seen in Figure 5A, while the equivalent comparison between the SPSP-PINS pulse and the Standard-MB pulse is shown in Figure 5B. From this it can be seen that some regions that did not exhibit voids in the Standard-MB volume still suffered from decreased signal and using an SPSP pulse could increase sensitivity in those areas. This is most evident in the sixth row, despite these slices being excluded from ROI-1 in the quantitative analysis. It is evident from Figure 5 that both SPSP pulses perform similarly well in recovering signal, with no obvious variations between their recovery patterns. Comparable results were observed for all subjects in the study, although there was significant variation between subjects with respect to the volume of voxels that suffered from signal loss. This is expected, as the signal loss artifact is largely dependent upon the anatomy of the individual subject. Although not shown here, there were no significant decreases in signal due to the use of an SPSP pulse.

fMRI Results

Figure 6 shows the breath-hold BOLD activation across the entire brain of subject 1 (top) and subject 4 (bottom) using the Standard-MB (A, D), SPSP-MB (B, E), and SPSP-PINS (C, F) pulses. The solid blue lines encompass manually selected regions where the use of SPSP-SMS pulses resulted in significant increases in the number of activated voxels. Even with visual inspection alone, it can be seen that the SPSP-SMS pulses significantly increase the activation coverage compared with the Standard-MB pulse, particularly in subject 1. It is noteworthy that these regions extend beyond the data-driven definition of ROI-1 (see Fig. 4). Examining Figure 5 reveals that this is not completely unexpected, although neither Figure 4 nor Figure 5 alone would have predicted the broad scope of the region of recovery in subject 1. Relatively speaking, the SPSP-MB pulse data exhibited higher activation coverage in ROI-1 than the SPSP-PINS data.

Table 2 shows the changes in activation coverage for both SPSP-SMS pulses in both ROIs calculated for all subjects. On average, both SPSP-SMS pulses increased the coverage in ROI-1 with 26.4% for SPSP-MB and 20.3% for SPSP-PINS. The increase in fMRI sensitivity in ROI-1 was accompanied by slightly decreased sensitivity in ROI-2, 2.6% for the SPSP-MB pulse, and 5.7% for the SPSP-PINS pulse, although two of the SPSP-MB

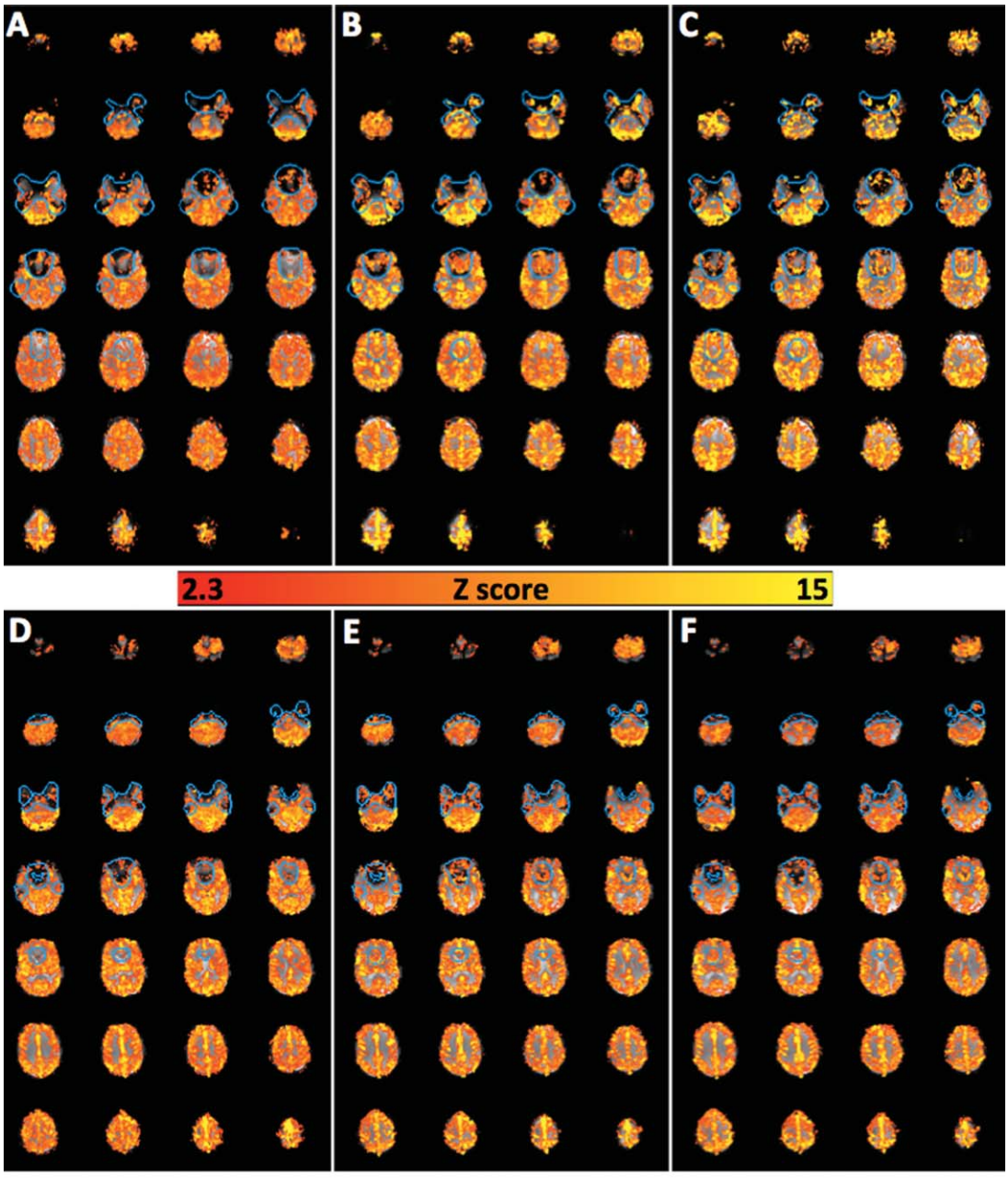

FIG. 6. Comparison of the breath-hold BOLD fMRI activation data for the images excited with Standard-MB (**A,D**), SPSP-MB (**B,E**), and SPSP-PINS (**C,F**) pulses in subject 1 (top) and subject 4 (bottom). The manually defined blue lines designate areas were there is a noticeable increase in activation coverage when using the SPSP-SMS pulses. This figure indicates that the SPSP-SMS pulses can effectively recover lost BOLD activation signal in regions otherwise undetected in the Standard-MB pulse experiment. The first and last slice groups exhibited insignificant amount of activation and thus have been omitted.

pulse experiments did not see a significant decrease in ROI-2 sensitivity. Examples of both an increase (subject 1) and a decrease (subject 4) can be see in Figure 6B and 6E, respectively. The SPSP-PINS data showed a decrease in ROI-2 activation sensitivity consistently in all subjects.

SPSP-MB Pulse Slice Thickness Comparison

Figure 7 shows the comparison of signal recovery as a function of slice thickness for the $N=7$ SPSP-MB pulses, with the Standard-MB images in the left column and the corrected SPSP-MB images in the right. Only the seven slices that showed signal loss and subsequent recovery are shown. From this figure, it can be seen that the thinner slices show less through-plane signal loss compared with the thicker slices as expected. The degree of signal loss is roughly proportional to the slice thickness, in particular for the more superior slices with signal loss in the frontal brain. Using the signal recovery analysis described above, subject-averaged signal recoveries of 39%, 37%, 40%, 41%, 37%, and 44% were found for

Table 2
Change in Percent of Each ROI that Comprises Activated Voxels with Z Value >2.3 for the Two SPSP-SMS Pulses Versus the Standard-MB Pulse

	Subject				Weighted Average
	1	2	3	4	
SPSP-MB					
ROI-1	38.5	19.2	15.3	21.3	26.4
ROI-2	3.4	0.7	−8.0	−6.6	−2.6
SPSP-PINS					
ROI-1	28.0	14.9	12.2	18.0	20.3
ROI-2	−3.6	−4.1	−6.2	−9.3	−5.7

2.5-, 3-, 3.5-, 4-, 4.5-, and 5-mm slice thicknesses, respectively. Although the thinner slices did show decreased signal loss and subsequently less recovered pixels, the SPSP-MB pulse still provided approximately the same percent improvement for all slice thicknesses. We therefore surmise that improvements in BOLD sensitivity similar to those reported here will be seen in experiments with thinner slices, with the main difference being that the ROI will be smaller. It should be further noted that visual inspection indicates that the SPSP-MB image quality for all thicknesses is comparable, indicating that using thicker slices is a viable option for fMRI experiments that were previously made impractical by the severity of the artifact.

DISCUSSION AND CONCLUSIONS

We have presented two alternative SPSP-SMS pulse methods for correcting susceptibility induced signal loss in SMS acquisitions. Both methods were shown to recover approximately 45% of the regions of signal dropout in volumes consisting of thirty-six $2.5 \times 2.5 \times 5$ mm^3 resolution slices. We also investigated how such pulses perform in the context of breath-holding BOLD fMRI. It was shown that susceptibility artifact-corrected fMRI data could be acquired at a rate of approximately three volumes per second, enabling future fMRI studies of the frontal lobe and nearby regions with high temporal resolution. The ability for SPSP pulse methods to provide whole brain signal loss compensation with little time penalty is a major advantage over the gradient based z-shim methods. The increased length of the SPSP pulses compared with the Standard-MB pulse, however, may increase the minimum TE values. This could also limit the bandwidth or resolution of the readout scheme, as 96×96 was the highest matrix size attainable for the 2D EPI sequence used in this study. Larger matrix sizes could, however, be easily achieved via in-plane undersampling at the expense of some slice acceleration so as to keep the total acceleration factor within the capabilities of the receiver array. It was also seen that SPSP pulses seem to be equally effective in recovering signal in thick slices as well as thinner ones.

Both pulses were demonstrated to be effective at recovering lost signal in the whole brain and were also demonstrated to significantly increase the number of activated voxels in regions corrupted by signal loss. To our knowledge, this is the first known demonstration of the use of SPSP pulses (single-slice or multislice) for providing an increase in BOLD activation. Although an increase in activation was observed, both pulses experienced some small losses in fMRI sensitivity in the rest of

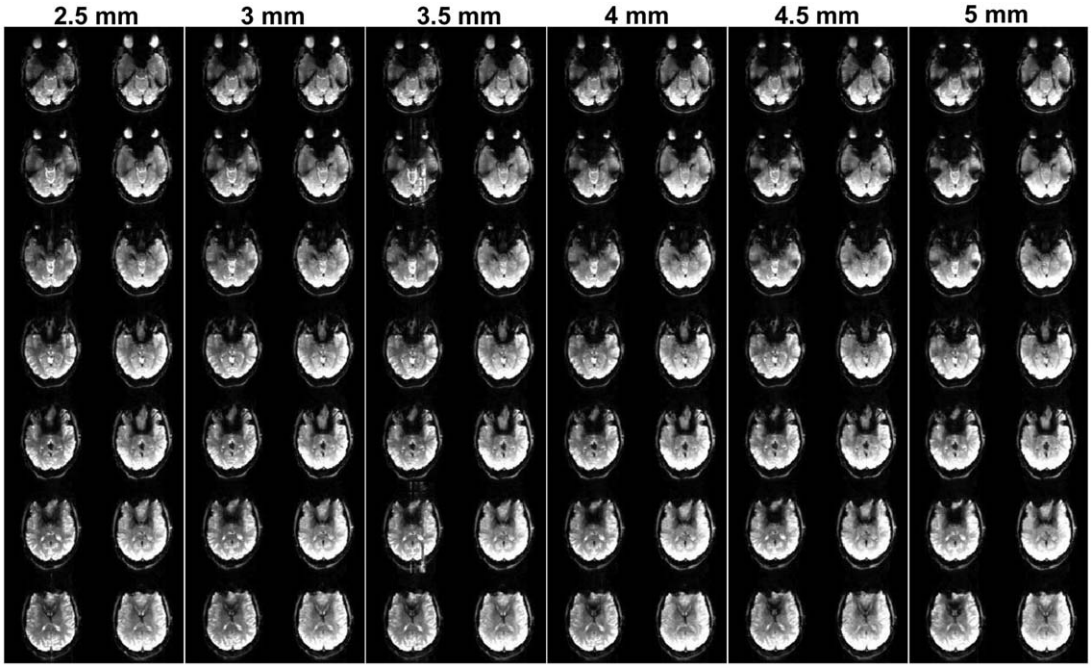

FIG. 7. Comparison of signal recovery as a function of slice thickness for an $N = 7$ SPSP-MB pulse. The uncorrected Standard-MB images are in the left-hand columns while the corrected SPSP-MB images are in the right-hand columns. Only the slices that showed signal loss and subsequent recovery are shown. Recovery is clearly visible even in the 2.5-mm slices. All of the slice thicknesses show comparable image quality.

the brain in some of the subjects. The cause of these losses is not known at this point, but we speculate that the pulse may cause unwanted dephasing in these regions, possibly due to deviation from the linear approximation between susceptibility gradient and frequency. Separate experiments mapping the temporal signal-to-noise ratio of the three pulses (data not shown) indicated that for the SPSP pulses there is no general loss in the quality of the signal with time compared with the Standard-MB pulse and show significant improvement in the areas of signal drop-out. These losses in BOLD sensitivity in ROI-2, however, were not as localized as the gains in ROI-1, and therefore will be useful for studies that simultaneously look for activation of the frontal lobe and any other region in the brain. Furthermore, it should be reiterated that two of the four subjects experienced no statistically significant loss when using the SPSP-MB pulse.

In situations where peak RF pulse voltage and SAR are a concern, or where high FAs need to be achieved by the correcting SPSP pulse, SPSP-PINS pulses have a distinct advantage over SPSP-MB pulses. In this study, the applied peak voltage on the Siemens scanner's body RF coil that achieved FA = 37° was 222 V, 263 V, and 75 V for Standard-MB, SPSP-MB, and SPSP-PINS, respectively. Moreover, the system voltage limits of 458 V would not have allowed for Standard-MB excitations above 77° and SPSP-MB excitations above 65°, while FA = 230° could be achieved in practice with SPSP-PINS pulses, if so necessitated by the experiment. In general, PINS pulses are fundamentally constrained by the ratio of the slice separation to slice thickness and may be found to be rather constrictive in applications where this ratio needs to be large. A second drawback of the PINS design is that head and coil dimensions are needed to restrict the number of slices. This is more problematic for an axial excitation as proposed here for through-plane signal loss compensation. We did observe some additional slice aliasing artifact with the SPSP-PINS pulse compared with the SPSP-MB pulse. For the sake of simplicity, the SPSP-PINS pulse was reconstructed with the $N = 9$ single-slice reference images. It is possible that reconstruction with a larger number of reference slices will decrease the aliasing artifact, particularly from the neck regions, increasing the SPSP-PINS pulse performance to a level more on par with the SPSP-MB pulse. Doing this would not directly penalize the fMRI experiment, and the only consequences are the time needed to acquire any additional reference slices and the corresponding fractional increase in the time to run the reconstruction algorithm.

It is worthwhile to consider how the SPSP methods presented here might be applied at higher fields such as 7T. One can expect approximately 7/3 more signal dephasing in a slice at 7T compared with that at 3T, because the variation in phase across a slice is linearly proportional to B_0. Therefore, to match performance at 3T, the 7T pulse parameters will need to be scaled by the same factor. For example, TE and subpulse length all need to be divided by 7/3. Shorter subpulses contribute to a shorter total pulse length, which is advantageous for the addressing the issue of the decreased TE. The primary concern, however, is that shorter subpulses are now needed to excite a sufficient number of thinner simultaneous slices. This may be challenging due to hardware limitations, including gradient peak and slew rate, RF sampling resolution, and peak B1 values. A compromise with the other pulse performance parameters will likely be needed. The application of SPSP-SMS pulses to higher field will be addressed in future work.

REFERENCES

1. Larkman DJ, Hajnal JV, Herlihy AH, Coutts GA, Young IR, Ehnholm G. Use of multicoil arrays for separation of signal from multiple slices simultaneously excited. J Magn Reson Imaging 2001;13:313–317.
2. Moeller S, Yacoub E, Olman CA, Auerbach E, Strupp J, Harel N, Ugurbil K. Multiband multislice GE-EPI at 7 Tesla, with 16-fold acceleration using partial parallel imaging with application to high spatial and temporal whole-brain fMRI. Magn Reson Med 2010;63:1144–1153.
3. Feinberg DA, Moeller S, Smith SM, Auerbach E, Ramanna S, Glasser MF, Miller KL, Ugurbil K, Yacoub E. Multiplexed echo planar imaging for sub-second whole brain FMRI and fast diffusion imaging. PLoS One 2011;5:e15710.
4. Setsompop K, Gagoski BA, Polimeni JR, Witzel T, Wedeen VJ, Wald LL. Blipped-controlled aliasing in parallel imaging for simultaneous multislice echo planar imaging with reduced g-factor penalty. Magn Reson Med 2012;67:1210–1224.
5. Feinberg DA, Yacoub E. The rapid development of high speed, resolution and precision in fMRI. NeuroImage 2012;62:720–725.
6. Hu X, Le TH, Parrish T, Erhard P. Retrospective estimation and correction of physiological fluctuation in functional MRI. Magn Reson Med 1995;34:201–212.
7. Norris DG, Koopmans PJ, Boyacioglu R, Barth M. Power independent of number of slices radiofrequency pulses for low-power simultaneous multislice excitation. Magn Reson Med 2011;66:1234–1240.
8. Frahm J, Merboldt K-D, Hanicke W. The influence of the slice-selection gradient on functional MRI of human brain activation. J Magn Reson B 1994;103:91–93.
9. Merboldt K-D, Finsterbusch J, Frahm J. Reducing inhomogeneity artifacts in functional MRI of human brain activation-thin slices vs gradient compensation. J Magn Reson 2000;145:184–191.
10. Wilson JL, Jezzard P. Utilization of an intra-oral diamagnetic passive shim in functional MRI of the inferior frontal cortex. Magn Reson Med 2003;50:1089–1094.
11. Song AW. Single-shot EPI with signal recovery from the susceptibility-induced losses. Magn Reson Med 2001;46:407–411.
12. Deng W, Yang C, Alagappan V, Wald LL, Boada FE, Stenger VA. Simultaneous z-shim method for reducing susceptibility artifacts with multiple transmitters. Magn Reson Med 2009;61:255–259.
13. Stenger VA, Boada FE, Noll DC. Three-dimensional tailored RF pulses for the reduction of susceptibility artifacts in T2*-weighted functional MRI. Magn Reson Med 2000;44:525–531.
14. Yip CY, Yoon D, Olafsson V, Lee S, Grissom WA, Fessler JA, Noll DC. Spectral-spatial pulse design for through-plane phase precompensatory slice selection in T2*-weighted functional MRI. Magn Reson Med 2009;61:1137–1147.
15. Yang C, Deng W, Alagappan V, Wald LL, Stenger VA. Four-dimensional spectral-spatial RF pulses for simultaneous correction of B1+ inhomogeneity and susceptibility artifacts in T2*-weighted MRI. Magn Reson Med 2010;64:1–8.
16. Yang C, Deng W, Stenger VA. Simple analytical dual-band spectral-spatial RF pulses for B1+ and susceptibility artifact reduction in gradient echo MRI. Magn Reson Med 2011;65:370–376.
17. Yang C, Poser BA, Deng W, Stenger VA. Spectral decomposition of susceptibility artifacts for spectral-spatial radiofrequency pulse design. Magn Reson Med 2012;64:1905–1910.
18. Pauly J, Nishimura D, Macovski A. A K-space analysis of small-tip-angle excitation. J Magn Reson 1989;81:43–56.
19. Meyer CH, Pauly JM, Macovskiand A, Nishimura DG. Simultaneous spatial and spectral selective excitation. Magn Reson Med 1990;15:287–304.
20. Block W, Pauly J, Kerr A, Nishimura D. Consistent fat suppression with compensated spectral-spatial pulses. Magn Reson Med 1997;38:198–206.

21. Pauly J, Cunningham C, Daniel B. Independent dual-band spectral-spatial pulses. In Proceedings of the 11th Annual Meeting of ISMRM. Toronto, Canada, 2003. p. 966.
22. Griswold MA, Jakob PM, Heidemann RM, Nittka M, Jellus V, Wang J, Kiefer B, Haase A. Generalized autocalibrating partially parallel acquisitions (GRAPPA). Magn Reson Med 2002;47:1202–1210.
23. Jenkinson M, Beckmann CF, Behrens TE, Woolrich MW, Smith SM. FSL. Neuroimage 2012;62:782–790.
24. Woolrich MW, Jbabdi S, Patenaude B, Chappell M, Makni S, Behrens T, Beckmann C, Jenkinson M, Smith SM. Bayesian analysis of neuroimaging data in FSL. Neuroimage 2009;45(suppl. 1):S173–S186.
25. Smith SM, Jenkinson M, Woolrich MW, Beckmann CF, Behrens T, Johansen-Berg H, Bannister PR, De Luca M, Drobnjak I, Flitney DE. Advances in functional and structural MR image analysis and implementation as FSL. Neuroimage 2004;23(suppl. 1):S208.
26. Jenkinson M, Smith S. A global optimisation method for robust affine registration of brain images. Med Image Anal 2001;5:143–156.
27. Jenkinson M, Bannister P, Brady M, Smith S. Improved optimization for the robust and accurate linear registration and motion correction of brain images. Neuroimage 2002;17:825–841.
28. Smith SM. Fast robust automated brain extraction. Hum Brain Mapp 2002;17:143–155.
29. Woolrich MW, Ripley BD, Brady M, Smith SM. Temporal autocorrelation in univariate linear modeling of FMRI data. Neuroimage 2001; 14:1370–1386.
30. Worsley K. Statistical analysis of activation images. Functional MRI: an introduction to methods 2001;14:251–270.